Computers Math. Applic. Vol. 17, No. 11, pp. 1455–1466, 1989
Printed in Great Britain.

0097-4943/89 $3.00 + 0.00

APPLYING THE LIFTING SURFACE METHOD TO THE BLADE TIP OF A HOVERING HELICOPTER

A. ISSER and A. ROSEN
Department of Aeronautical Engineering, Technion, Israel Institute of Technology, Haifa 32000, Israel

(*Received* 13 *June* 1988)

Abstract—The approach of inner/outer fields is applied in order to calculate the aerodynamic loads at a blade tip (inner field) of a helicopter in hovering or axial flight. It is shown that if the inner field includes the wake in the vicinity of the tip region, then the well known lifting surface method for fixed wings can be applied in order to study the aerodynamic field at the tip. This method is more efficient than other methods that have been previously applied and thus it is suitable for repeated analyses during the design procedure. Furthermore, the method is capable of dealing with complicated tip geometries without requiring excessive computer resources. Examples of using the method are presented, where the calculated results are compared with experimental ones.

1. INTRODUCTION

A significant effort has been devoted during recent years in order to study the aerodynamic behavior of helicopter blades' tips. References [1–11] are representative examples of this effort. The reasons for this extensive research are twofold: first, the blade tip, with its relatively high velocities, presents a very important contribution to the rotor thrust. Therefore, any improvement in the aerodynamics of the tip will result in an important improvement to the net rotor performance. On the other hand, the aerodynamic behavior at the tip is much more complicated than the behavior at other regions of the flow field. This complexity is the result of: inherent three-dimensional nature of the flow, high velocities and therefore important compressibility effects, complicated influences of the returning wake and relatively complicated geometries of blade tips.

Because of the complexity of the flow field at the blade tip, relatively complicated theoretical models have been developed in order to deal with this region properly. If such complicated models will be applied to solve the whole flow field of the rotor, enormous computer resources will be required in order to solve even a single case. On the other hand, it is possible to calculate the flow field at other regions of the rotor flow field, by using relatively simple models. Thus, in order to arrive at an efficient and accurate enough solution scheme, the idea of combining two different models seems attractive. Namely, the more complicated model is applied only to regions of the flow where it is required (the tip region), while a simpler model is applied to the rest of the flow field. It is clear that special care is required in order to combine the two models so that they will yield a final complete solution of the problem.

The above mentioned inner/outer domain concept has been applied by different researchers in order to calculate the aerodynamic behavior of helicopter blades [3, 7, 9, 11]. In all these studies the inner (more accurate) domain has been solved using finite difference schemes. It has been shown that by using appropriate finite difference meshes and appropriate tailoring between the inner and outer domains, very good results are obtained. On the other hand, as the refinement of the mesh is increased, the required computer resources for the solution of each case are enormously increased.

The present paper will present a method where the inner/outer domain concept is applied in order to calculate the aerodynamic loads at the blade tip of a hovering rotor (or a rotor in a slow axial motion). The solution of the flow field at the inner domain (the tip region) is obtained using the lifting surface method. The model can cope very easily with any tip geometry. The influence of the outer domain on the tip region is introduced through velocities which are induced by the outer domain over the tip region. A requirement of continuity in the load distribution along the blade, while passing from one domain to the other, is also applied.

After the derivation of the new model, it will be applied to calculate the aerodynamic load at the tip region of different blades. The theoretical results will be compared with experimental ones.

The present method is very efficient, compared to other methods, for analysing the aerodynamic behavior of different blade tips at different hovering or axial flight conditions. Thus it may be useful in the design process where a large number of analyses, of different designs, is required. While the present paper concentrates on the axisymmetric case (axial flight or hovering), extension to forward flight, which is an unsteady case, seems natural. The efficiency that the method may offer in this case is very attractive.

2. THEORETICAL DERIVATION

2.1. Basic assumptions and geometric description

The present paper deals with a helicopter rotor in hovering or slow axial flight. The derivation is based on the following assumptions:

(a) The flow field is subsonic, isentropic and inviscid.
(b) The blade surfaces slopes are small, relative to the incoming flow direction. The blade thickness is also small relative to its chord.
(c) The rotor is isolated and thus fuselage or ground influences are not taken into account.
(d) The aspect ratio of the blades is much greater than unity.
(e) The axial velocity of the rotor, V_c, is small compared to the blade tip velocity.
(f) The rotor rotates at a constant angular velocity Ω.
(g) For an observer on a rotating blade, the phenomenon is not a function of time, namely, steady.

The assumption of a subsonic flow (assumption a) deserves explanation. During recent years a significant effort (see the above mentioned references) has been devoted to the solution of transonic flows at blade tips. This problem is very important to the tip region of advancing blades of helicopters, moving at a high advance ratio. In the case of hovering or slow axial flight, transonic effects are much less important and can be neglected. Thus, the present efficient model is suitable for most practical purposes where a large number of configurations at different flight conditions are calculated.

The blade tip region is described in Fig. 1. x_1, y_1, z_1 is a dimensional Cartesian system of coordinates which rotates and moves axially with the rotor. z_1 coincides with the axis of rotation, y_1 is the spanwise coordinate, while x_1 points in the chordwise direction. x and z are nondimensional coordinates which are obtained after x_1 and z_1, respectively, are divided by a representative chord length l_c. The nondimensional spanwise coordinate y is obtained after y is divided by the disk radius, R. Dealing with the tip region, it is convenient to replace the coordinate y by another nondimensional spanwise coordinate, s, defined as follows:

$$s = (1 - y)R/l_c. \tag{1}$$

s equals to zero at the tip and increases while moving towards the blade root.

The projection of the blade leading edge onto the x–s plane is described by the curve $G(s)$, while the curve $Q(s)$ describes the projection of the trailing edge. The local nondimensionalized chord, $C(s)$, is thus

$$C(s) = Q(s) - G(s). \tag{2}$$

The upper and lower surfaces of the blades are $z_u(x, s)$ and $z_l(x, s)$, respectively. Since the blade is thin, it will be represented by its mid-surface, $z_m(x, s)$ (see Fig. 1.).

2.2. The lifting surface model

The flow field behind a rotating blade is shown in Fig. 2. As shown in the figure, the flow field is divided into four regions: S_1—the tip region of the blade; S_2—the near wake, just behind the tip region; S_3—the blade, excluding the tip region (S_1); and S_4—The whole wake, excluding S_2.

The cross section $s = s_i$ (see Fig. 1) marks the boundary between S_1 and S_3.

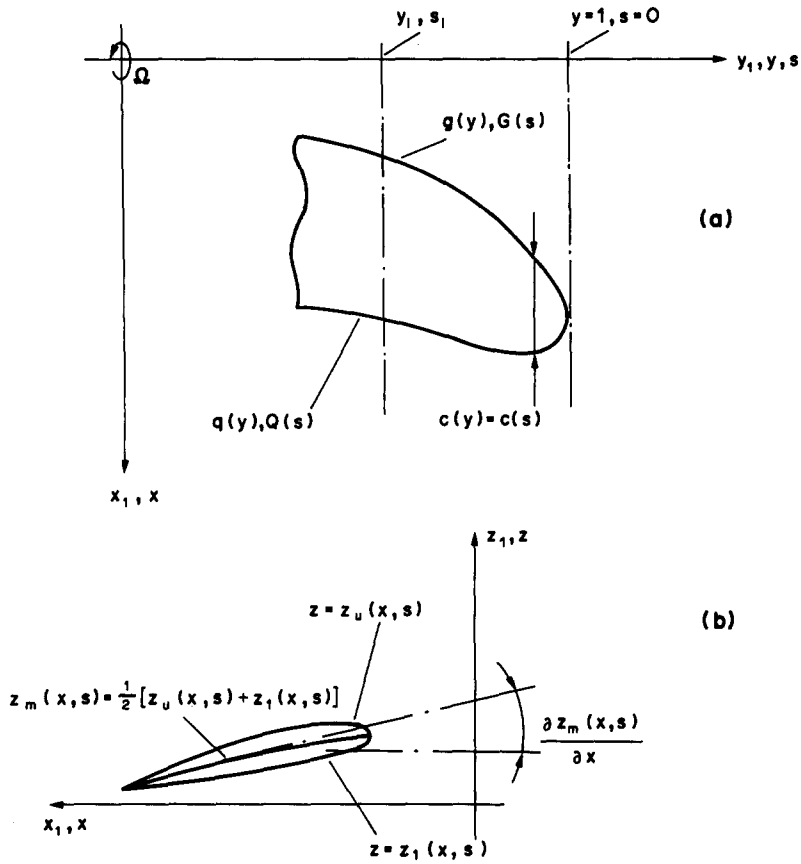

Fig. 1. General description of the blade tip. (a) Projection onto the x–s plane; (b) typical cross section in the x–z plane.

By using the lifting surface theory of rotary wings [12–17] it can be shown that for the axisymmetric steady case of hovering or axial motion, the axial component of the induced velocity at any point (x, s) over the blade can be described as follows:

$$v_i(x, s) = \iint_{(S_1 + S_3)} K(\xi, \eta, x, y, \beta)\Delta p(\xi, \eta)\, d\xi\, d\eta. \tag{3}$$

ξ and η are blade coordinates, equivalent to x and s, respectively. β is a compressibility factor, defined as

$$\beta = (1 - M_y^2)^{1/2}, \tag{4}$$

where M_y is the Mach number at the cross section y of the blade. Δp is the local pressure difference (between the lower and upper surfaces of the blade).

The kernel $K(\xi, \eta, x, y, \beta)$ is obtained by integration along a streamline, starting far downstream, and finishing at the point (ξ, η) of the blade:

$$K(\xi, \eta, x, y, \beta) = \int_{-\infty}^{\sigma_0} K^*(\xi, \eta, x, y, \beta, \sigma)\, d\sigma. \tag{5}$$

σ is a running coordinate downstream, along the blade and the wake. It is convenient to consider σ as an azimuth angle measured along the wake (see Fig. 3). σ_0 is the coordinate of the point (ξ, η).

The boundary between regions S_1 and S_2 will be defined by σ^* (see Fig. 3). Substitution of equation (5) into (3) and separation between S_1 and S_3, imply

$$v_i(x, s) = v_{ie}(x, s) + v_{io}(x, s), \tag{6}$$

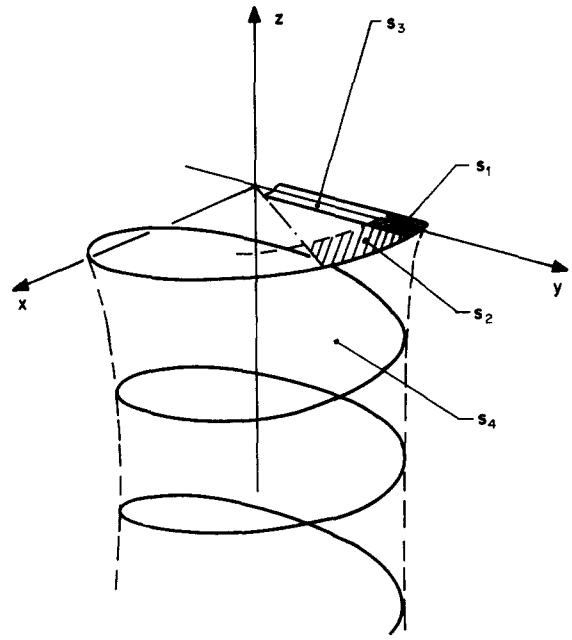

Fig. 2. The flow field behind a blade.

where

$$v_{ie}(x, s) = \iint_{S_1} \left[\int_{\sigma^*}^{\sigma_0} K^*(\xi, \eta, x, y, \beta, \sigma)\, d\sigma \right] \Delta p(\xi, \eta)\, d\xi\, d\eta, \tag{7a}$$

$$v_{io}(x, s) = \iint_{S_1} \left[\int_{-\infty}^{\sigma_*} K^*(\xi, \eta, x, y, \beta, \sigma)\, d\sigma \right] \Delta p(\xi, \eta)\, d\xi\, d\eta + \iint_{S_3} \left[\int_{-\infty}^{\sigma_0} K^*(\xi, \eta, x, y, \beta, \sigma)\, d\sigma \right] \Delta p(\xi, \eta)\, d\xi\, d\eta. \tag{7b}$$

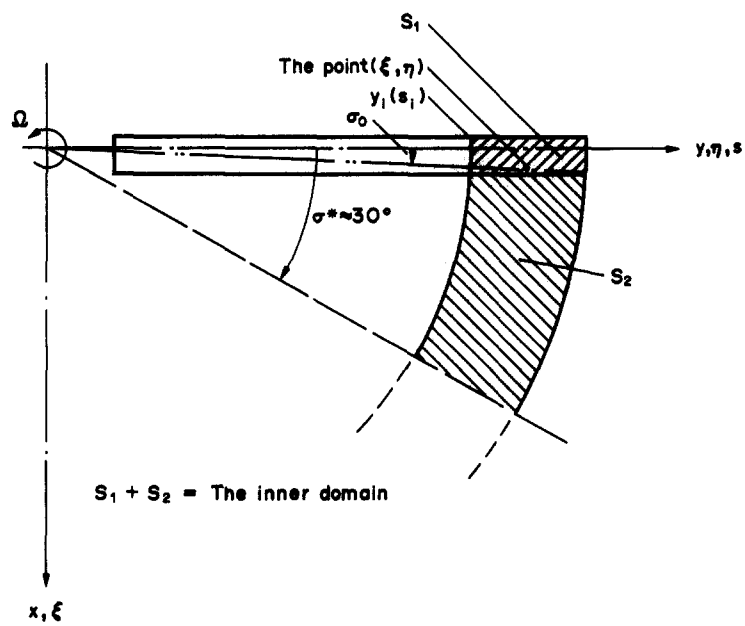

Fig. 3. The near wake behind the blade tip.

$(S_1 + S_2)$ is defined as the inner domain. $(S_3 + S_4)$ is the outer domain. v_{ie} is the contribution of the inner domain to the induced velocity in this domain itself. This part includes the singular integral typical of all lifting surface models. v_{io} is the contribution of the outer domain.

It can be shown that if σ^* is taken equal to 30° (see Fig. 3), and taking into account the fact that the axial displacement of the wake in the inner region is small, then v_{ie} can be approximated as (detailed derivation appears in [18])

$$v_{ie}(x, s) = \frac{U_r}{8\pi} \int_{s'=0}^{s'=s_i} \int_{x'=G(s')}^{x'=Q(s')} l(x', s') \left(1 + \frac{x - x'}{[(x - x')^2 + \beta_r^2 (s - s')^2]^{1/2}}\right) \frac{dx'\, ds'}{(s - s')^2}. \tag{8}$$

$l(x, s)$ is a nondimensional load defined as

$$l(x, s) = \Delta p(x, s)/(\tfrac{1}{2}\rho_\infty U_r^2). \tag{9}$$

Based on the present assumptions, the incoming flow velocity varies in a linear manner along the blade. If the tip region is relatively small, namely $[(s_i l_c/R) \ll 1]$, then it is possible to introduce a representative velocity U_r. U_r obtains some value between the magnitude of the incoming flow at the cross-section s_i and the tip. As it will be shown later, the influence of the choice of U_r on the results is usually negligible.

β_r is the compressibility factor based on U_r, namely

$$\beta_r^2 = 1 - M_r^2. \tag{10}$$

M_r is the Mach number based on the velocity U_r.

The integrand of equation (8) is identical to the integrand of the singular integral of the induced velocity according to the well known lifting surface theory of Multhopp [19]. This theory deals with a fixed wing in a uniform subsonic flow. While the boundaries of the integral in the case of a fixed wing include the whole wing, here the intergration is carried out only over the tip region. The fact that the equation for the tip region is equivalent to the equation of a fixed wing is not surprising if one recalls the results of Caradonna and Isom [1, 2]. They have shown that the differential equation of small disturbances at the tip region of a high aspect-ratio blade is identical to the equation of a fixed wing in a uniform flow, where the uniform flow velocity is taken equal to the flow velocity at the blade tip. A derivation similar to Ref. [2] is presented in [18], where it is shown that the same differential equation is applicable also to the case of a rotor in a slow axial flight.

The integral of equation (8) presents a singularity problem. This singularity has been investigated by different researchers (the interested reader will find a relevant list of references in [20]). Reference [20] presents a new efficient method to cope with this singularity. This method [20] will be used in the present calculations.

2.3. The boundary conditions

The boundary conditions are of two kinds. First there is the condition of nonpenetration of the flow through the blade surface. Second, the condition of continuity of the aerodynamic load while crossing the cross section $s = s_i$ (from the region S_1 to S_3), is also applied.

The condition of nonpenetration of the flow through the blade surface means that the flow close to the blade is tangent to the surface. As mentioned above (and as is usual in all lifting surface theories), the blade is replaced by its mid-surface $z_m(x, s)$. The condition is described by the following equation (small terms have been neglected based on the above described assumptions and the assumption of small disturbances):

$$-\Omega R(1 - s l_c/R) \frac{\partial z_m(x, s)}{\partial x} + v_i(x, s) - V_c = 0. \tag{11}$$

The last equation should be satisfied at any point (x, s) of the blade tip.

Substitution of equation (6) into (11), using (8) and dividing the equation by ΩR, imply

$$\alpha(x, s) = -\frac{1}{8\pi} \int_{s'=0}^{s'=s_i} \int_{x'=G(s')}^{x'=Q(s')} l(x', s') \left(1 + \frac{x - x'}{[(x - x')^2 + \beta_r^2 (s - s')^2]^{1/2}}\right) \frac{dx'\, ds'}{(s - s')^2}, \tag{12}$$

where

$$\alpha(x, s) = \frac{\Omega R}{U_r}\left(\tilde{v}_{io} - \tilde{V}_o - (1 - sl_c/R)\frac{\partial z_m}{\partial x}\right). \tag{13}$$

The wiggle indicates nondimensional velocities, obtained after dividing the dimensional velocities by (ΩR). A solution of the integral equation [as presented by equation (12)] gives the aerodynamics of the inner domain. The solution yields the unknown function $l(x, s)$. While solving the inner domain aerodynamics, $\alpha(x, s)$ [as defined by equation (13)] can be considered as a known input. According to (13), $\alpha(x, s)$ is a function of: (a) the influence of the outer domain through the induced velocity $\tilde{v}_{io}(x, s)$; and (b) the geometry of the blade's tip (z_m), and the flight condition. $\tilde{v}_{io}$ is obtained by a solution of the outer domain. As indicated above, the solution may be obtained using different methods which are not necessarily as accurate as the inner domain model.

3. THE SOLUTION TECHNIQUE

The nondimensional load, $l(x, s)$, is described by the following double series:

$$l(x, s) = \frac{1}{C(s)}\sum_{n=0}^{N_0}\sum_{m=1}^{M_0} a_{nm}h_n(x)e_m(s). \tag{14}$$

$h_n(x)$ are chordwise shape functions of the aerodynamic load. The series should include the leading edge singularity and satisfy the Kutta condition. $e_m(s)$ are the spanwise shape functions that satisfy the condition of zero load at the tip $s = 0$. It is clear that for an exact solution the series should be infinite, but for practical purposes they are finite with $(N_0 + 1)$ chordwise shape functions and M_0 spanwise functions. Thus, the unknowns of the problem become the $[(N_0 + 1) \times M_0]$ coefficients a_{nm}.

Substitution of equation (14) into (12) implies

$$\alpha(x, s) = \sum_{n=0}^{N_0}\sum_{m=1}^{M_0} a_{nm}\alpha'(x, s, n, m), \tag{15}$$

where

$$\alpha'(x, s, n, m) = -\frac{1}{8\pi}\int_{s'=0}^{s'=s_i}\int_{x'=G(s')}^{x'=Q(s')} f_n(x)e_m(s)\left(1 + \frac{x - x'}{[(x - x')^2 + \beta_r^2(s - s')^2]^{1/2}}\right)\frac{dx'\,ds'}{(s - s')^2}. \tag{16}$$

Any point (x, s) is associated with $[(N_0 + 1) \times M_0]$ coefficients $\alpha'(x, s, n, m)$. The calculation of these coefficients includes the singularity problem. As already mentioned above, a recently developed efficient method [20] will be applied to the calculation of the coefficients. This method is capable of dealing with any geometry of the tip and any choice of the functions $f_n(x)$ and $e_m(s)$.

In general, equation (16) should be satisfied at any point of the tip region. Practically, the equation will be satisfied at a finite number of collocation points. The number of collocation points is N_c, where

$$N_c \geqslant (N_0 + 1)M_0. \tag{17}$$

In a case where the equilibrium sign in equation (17) holds, the number of unknowns is equal to the number of equations. In all other cases an overdetermined system of equations is obtained, and solved by applying least squares methods [21].

The final set of equations can be described by the following matrix notation:

$$\{\alpha\} = [K]\{a\}. \tag{18}$$

$\{\alpha\}$ is a vector of order N_c which includes all the $\alpha(x, s)$ at the collocation points. $\{a\}$ is a vector of order $[(N_0 + 1) \times M_0]$, that includes the coefficients a_{nm}. The matrix $[K]$ has a dimension $\{N_c \times [(N_0 + 1)M_0]\}$ and its terms are the coefficients $\alpha'(x, s, n, m)$.

As mentioned above, except from the condition of nonpenetration of the flow through the blade surface, the condition of continuity of the aerodynamic load along the blade is also applied. In particular, this condition requires a continuity of the aerodynamic load at the cross section $s = s_i$,

while passing from the region S_1 to the region S_3. This condition can be applied in different ways, using different approaches. The application of this condition is also a function of the format of the outer domain solution. In the present paper the continuity condition will be imposed on the resultant cross-sectional lift. It is required that at the cross section $s = s_i$ the cross-sectional lift obtained by the inner domain solution will be equal to the cross-sectional lift obtained by the outer domain solution. This condition yields another equation which is added to the system of equations (18).

Thus, in summary, the solution of the tip region aerodynamics (inner domain) is obtained as follows: the outer domain solution is obtained first. This solution yields the induced velocities over the tip, $\tilde{v}_{io}(x, s)$, and the aerodynamic force at the cross section $s = s_i$. Based on $\tilde{v}_{io}(x, s)$ at the collocation points, the tip geometry ($Q(s)$, $G(s)$, $\partial z_m/\partial x$) and the flight condition (ΩR, V_c), the vector $\{\alpha\}$ is assembled. Then by solving equation (18) (adding also the boundary condition at $s = s_i$) the vector of unknowns $\{a\}$ is calculated. If the matrix $[K]$ is known, relatively small computer resources are required to obtain a solution. For a certain tip geometry of a rotor operating at a certain tip Mach number, the matrix $[K]$ is calculated once and stored. Thus calculations for different operating conditions (different V_c, pitch angle and twist) are very quick and do not require large computing resources.

4. NUMERICAL EXAMPLES

The outer domain solution is used as an input to the inner domain solution. Any appropriate method can be used in order to solve the outer domain problem. In the present section, a recently developed vortex lattice (VLM) free wake analysis [22, 23] is used in order to solve the outer domain problem. This analysis yields $v_{io}(x, s)$ at the collocation points and the aerodynamic load at the cross section $s = s_i$.

The chordwise shape functions, $h_n(x)$, are identical to the shape functions that were used by Wagner [24, 25]. There are different ways of expressing these functions, one of which is

$$h_n(\psi) = (2/\pi)\left(\operatorname{cotan}(\psi/2) - 2\sum_{k_1=1}^{n} \sin(k_1\psi)\right), \tag{19a}$$

$$\cos\psi = 1 - 2X, \tag{19b}$$

$$X = [x - G(s)]/C(s). \tag{19c}$$

It can be seen that there is a normalization of the shape functions based on the local chord. Each term in the series contains the leading edge singularity and satisfies Kutta's condition at the trailing edge.

The spanwise shape functions have been chosen as follows:

$$e_m(s) = \begin{cases} \sin[\pi s/2s_i], & m = 1; \quad (20a) \\ \sin[\pi s(m-1)/s_i], & m > 1. \quad (20b) \end{cases}$$

As can be seen from equations (20), only the first term ($m = 1$) contributes to the load at the cross section $s = s_i$. This choice has been found to be very convenient when applying the boundary conditions. All the other terms have an influence inside the tip region and they also influence the load slope at the boundary cross section.

As already indicated above, $\alpha'(x, s, n, m)$ are calculated by using the method of [20]. In all the cases, the number of chordwise shape functions ($N_0 + 1$) will be equal to the number of chordwise collocation points, while the number of spanwise functions M_0 will be equal to the number of collocation cross sections. Thus, over determined cases will not be dealt with in the present examples.

Example I

The rotor and its operating conditions are identical to two experiments that were reported by Caradonna and Tung [6]. This is a two bladed rotor where the disk radius is 1.143 m and the

constant chord equals 0.1905 m. The cross-sectional pitch angle is constant along the blade and equals 8°. The aerodynamic profile of the blade is NACA 0012. The rotor was operating at two rotational velocities which resulted in tip Mach numbers of 0.44 and 0.6.

Three cases of different tip regions are considered:

(a) The tip region ranges from the cross section $y_i = 0.85$ to $y = 1.0$. There are seven collocation points along the blade, located at the cross sections $y = 0.87, 0.89, 0.91, 0.93, 0.95, 0.97, 0.99$. All the collocation points are located at the classical three quarters chord location ($X = 0.75$). In this case U_r is taken equal to $(0.925\,\Omega R)$.

(b) The tip region starts at $y_i = 0.90$. The collocation points are located at the following five cross sections: $y = 0.91, 0.93, 0.95, 0.97, 0.99$. At each cross section there are two collocation points at the "optimal" chordwise locations according to Multhopp [19], $X = 0.3455, 0.9045$. In this case U_r is taken equal to $(0.95\,\Omega R)$.

(c) The tip region starts at $y_i = 0.95$. There are four collocation cross sections, $y = 0.96, 0.97, 0.98, 0.99$. At each cross section there are two collocation points at $X = 0.3455, 0.9045$. U_r is taken equal to $(0.975\,\Omega R)$.

In Fig. 4 the lift coefficient distribution along the blade tip (when $M_T = 0.44$), as obtained from the above three cases, is presented. Results of the free wake VLM model, used as the outer domain [22, 23], are also presented for comparison. There are some differences between the three cases. These differences are larger near the cross section $s = s_i$ and they decrease rapidly (practically disappear) as the distance from $s = s_i$ increases. The results of the VLM free wake analysis are higher than the results of the present model. The experimental results are located between the VLM free wake model and the lifting surface.

Similar results to those presented in Fig. 4 have also been obtained for the case where $M_T = 0.6$.

In Fig. 5 the distribution of the nondimensional load, $l(x, y)$ is presented along two cross sections ($y = 0.89, 0.96$), for two rotational speeds ($M_T = 0.44, 0.6$). The agreement between the experimental and theoretical results is better for $M_T = 0.44$ compared with $M_T = 0.60$. The agreement is in general of the same quality for both cross sections, while in all the cases the agreement deteriorates near the leading edge.

In relation to the fact that the agreement is better for the case where $M_T = 0.44$, it should be noted that the present outer domain calculations do not include compressibility corrections. Including such corrections may improve the agreement in the case when $M_T = 0.6$.

It is worth mentioning that calculations of the three cases using other values of U_r have been carried out. In case (a) for example, values of $U_r = (0.85\,\Omega R)$ or $U_r = (1.0\,\Omega R)$ have been applied. Only negligible differences in the results have been observed.

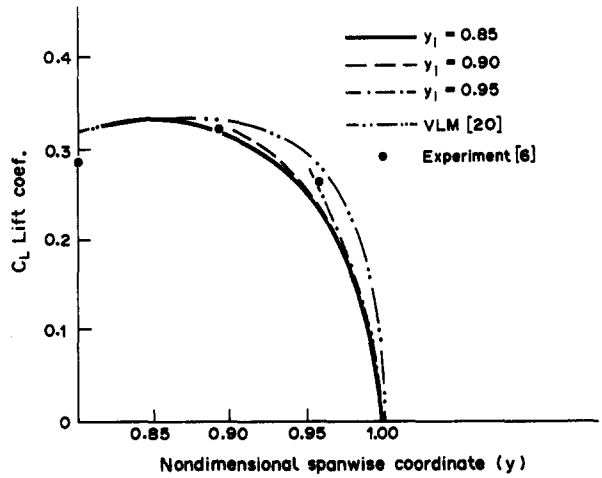

Fig. 4. Example I—lift coefficient distribution along the blade tip ($M_T = 0.44$).

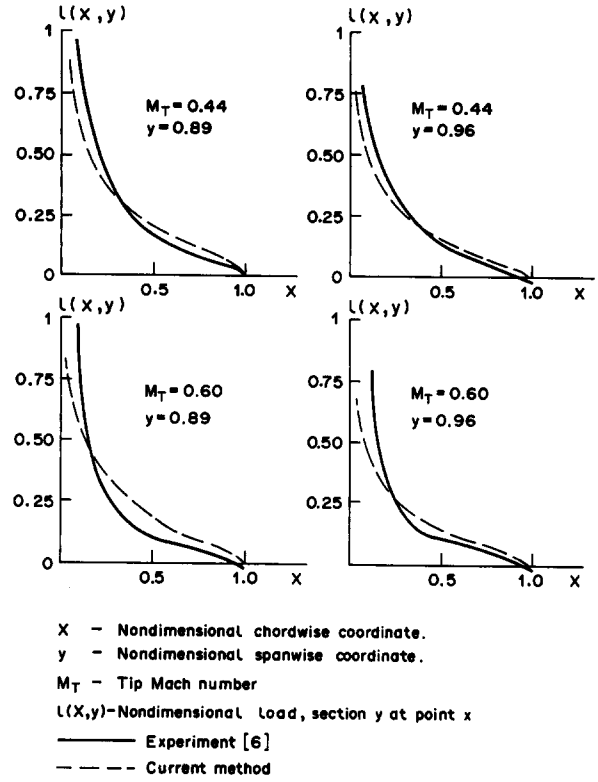

Fig. 5. Example I—aerodynamic load distribution at different cross sections of the blade tip ($M_T = 0.44, 0.6$).

Example II

This is a rotor similar to that of Example I. The rotor has two blades with constant chord and pitch. The tip Mach number is 0.6. The main difference between this example and the former one lies in the aspect ratio of the blades. While in Example I the aspect ratio (R/C) is 6.0, here it equals 13.7. In [7] experimental results for Example II are presented.

In Fig. 6 the lift coefficient distribution is presented for cases where $y_i = 0.85, 0.90, 0.95$. The calculations are compared with experimental results. The behavior is similar to that of Fig. 4. The theoretical results are lower than the experimental ones.

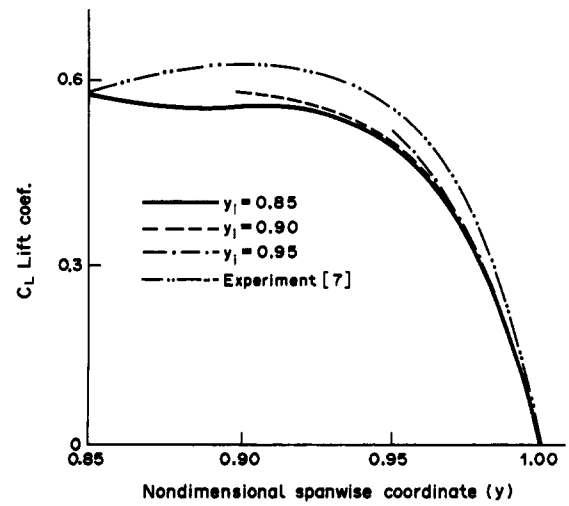

Fig. 6. Example II—lift coefficient distribution along the blade tip ($M_T = 0.6$).

Example III

This example presents one of the main advantages of the present model which allows an easy and accurate description of any complicated tip geometry. The blade that will be considered has an ogee tip. In [4] experimental results for blades with ogee tip are presented. The tip geometry, as given in [4], is presented in Fig. 7. The rotor has two blades, the disk radius is 1.05 m and the constant chord (excluding the tip region) is equal to 0.0762 m. The pitch angle at the root equals 17.8° and it drops linearly towards the tip, where the pitch difference between the root and the tip equals $-10.7°$. The rotor speed is $\Omega = 73.3$ (rad/s), yielding a tip Mach number of 0.226.

The outer domain solution is obtained by the previously mentioned VLM free wake model. An accurate description of the ogee shape by the VLM method will require a very fine mesh of the tip region, and consequently will require extremely high computational resources. Therefore, while solving the outer domain problem, the tip is described as a triangular one, also shown in Fig. 7. Except for the solution of the outer region, the triangular tip will also be solved for comparison purposes.

The inner domain solutions include three cases:

(a) A triangular tip region that begins at $y_i = 0.9$. There are 18 collocation points located at nine cross sections along the tip (see Fig. 7).
(b) A triangular tip region that starts at $y_i = 0.95$. There are four collocation cross sections inside this region, where each cross section has two collocation points.
(c) An ogee tip region where $y_i = 0.9$. There are 18 collocation points inside this region.

The circulation distribution along the blade is shown in Fig. 8, for the above described three cases, the outer domain VLM solution and experimental results [4]. The outer domain VLM analysis results show a significant deviation in comparison with the experimental results. The results

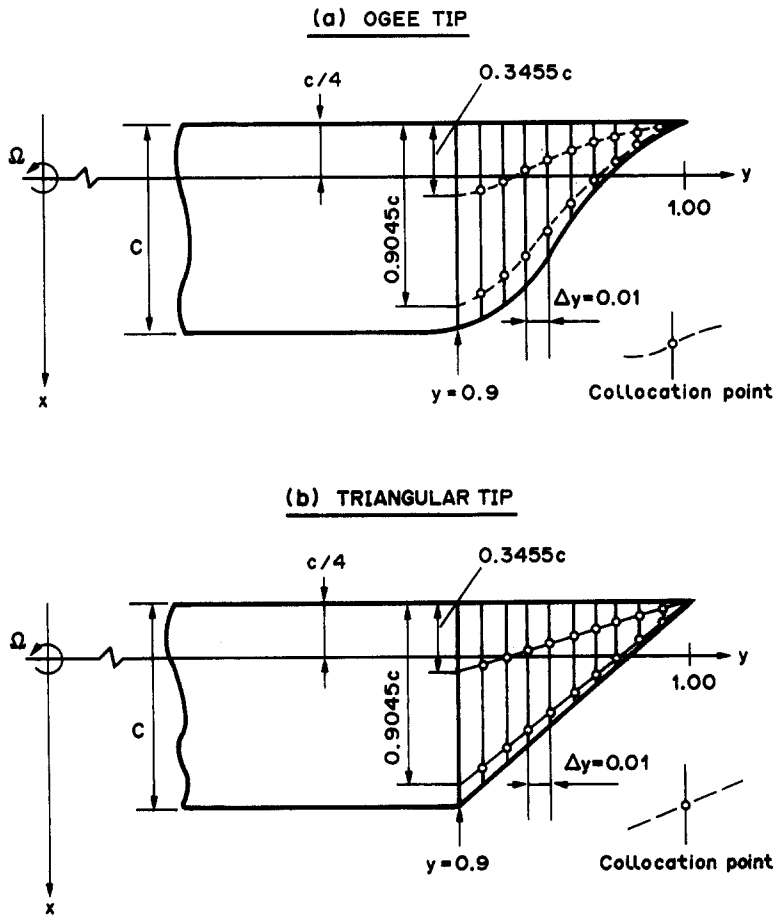

Fig. 7. Example III—tip geometry and collocation points distribution: (a) ogee tip, (b) triangular tip.

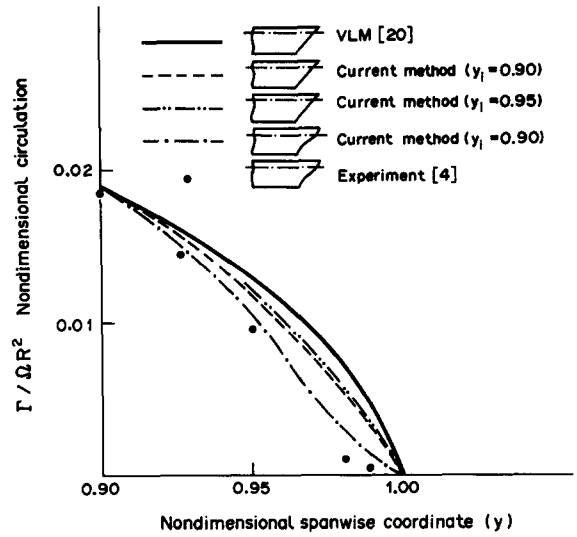

Fig. 8. Example III—circulation distribution along the blade tip.

of cases (a) and (b) (lifting surface, triangular tip shape) are very close and again prove the relatively low sensitivity of the method to the choice of the cross section s_i. Still, the results of cases (a) and (b) are noticeably higher than the experimental results. The results of case (c), where the accurate shape of the ogee tip is considered, show very nice agreement with the experimental results. It is worth emphasizing here that while using the present lifting surface method, in contrast to other methods, taking into account the accurate tip geometry (it holds to any geometry and not only the ogee tip) does not result in any meaningful increase in the computational effort.

This example presents the advantages of using a fairly crude model for the outer field and a more refined model for the inner solution at the tip.

5. CONCLUSIONS

A new method, where the inner/outer domain approach is used in order to calculate the aerodynamic loads at the tip of a hovering helicopter blade, has been presented. The solution of the inner domain is based on using the lifting surface method.

There are two main advantages associated with the new method:

(a) Compared to other methods, it is very efficient concerning computer resources. Thus it allows many computations associated with different pitch angles and axial velocity combinations.
(b) Without any significant increase in the solution effort, it is possible to deal with complicated tip geometries.

Based on the above described results it seems that it will be interesting to investigate the use of the new method using different outer domain solutions (in addition to the presently used VLM free wake analysis). Of special interest will be the use of outer domain models that include compressibility corrections. It also seems attractive to extend the present method to cases of forward flight, where efficiency is very important.

Acknowledgement—The authors would like to than Mrs B. Hirsch for typing the manuscript.

REFERENCES

1. F. X. Caradonna and M. P. Isom, Subsonic and transonic potential flow over helicopter rotor blades. *AIAA J.* **10**, 1606–1612 (1972).
2. M. P. Isom, Unsteady subsonic and transonic potential flow over helicopter rotor blades. NASA-CR-2463 (1974).
3. R. Arieli and M. E. Tauber, Analysis of the quasi-steady flow about an isolated lifting helicopter rotor blade. *JIAA* August TR-24 (1979).
4. J. D. Ballard, K. L. Orloff and A. Laebs, Effect of tip shape on blade loading characteristics and wake geometry for a two-bladed rotor in hover. *J. Am. Helicopter Soc.* **25**(1), 30–35 (1980).

5. B. Maskew, Influence of rotor blade tip shape on tip vortex shedding—an unsteady, inviscid analysis. *Proc. 36th Annual Forum American Helicopter Society*, Washington, D.C., Paper No. 6 (1980).
6. F. X. Caradonna and C. Tung, Experimental and analytical studies of a model helicopter rotor in hover. *6th European Rotorcraft Forum*, Bristol, England, Paper No. 25 (1980).
7. F. X. Caradonna, A. De Sopper and C. Tung, Finite difference modeling of flows including wake effects. *8th European Rotorcraft Forum*, Aix-En-Provance, France, Paper No. 2.7 (1982).
8. J. J. Philippe and A. Vuillet, Aerodynamic design of advanced rotors with new tip shapes. *Proc. 34th Annual Forum American Helicopter Society*, St. Louis, Mo., pp. 58–71 (1983).
9. T. A. Egolf and S. P. Sparks, Hovering rotor airloads prediction, using full potential flow analysis with realistic wake geometry. *Proc. 41st Annual Forum American Helicopter Society*, Ft. Worth, Tex. (1985).
10. A. De Sopper, Study of the unsteady transonic flow on rotor blades with different tip shapes. *Vertica* **9**, 257–272 (1985).
11. F. X. Caradonna and C. Tung, A review of current finite difference rotor flow methods. *Proc. 42nd Annual Forum American Helicopter Society*, Washington, D.C., pp. 967–983 (1986).
12. J. J. Costes, Computation of unsteady aerodynamic forces on helicopter rotor blades. NASA-TT-F-15039 (1973).
13. R. Dat, Aeroelasticity of rotary wing aircraft. AGARD Lecture Series No. 63, pp. 4.13–4.33 (1973).
14. D. B. Hanson, Compressible helicoidal surface theory for propeller aerodynamics and noise. *AIAA J.* **21**, 881–889 (1983).
15. W. Z. Stepniewski and C. N. Keys, *Rotary Wing Aerodynamics*. Dover, New York (1984).
16. D. B. Hanson, Compressible lifting surface theory for propeller performance calculation. *J. Aircraft* **22**, 19–27 (1985).
17. H. L. Runyan and T. Hasiang, Application of a lifting surface theory for a helicopter in forward flight. *11th European Rotorcraft Forum*, London, England, Paper No. 24 (1985).
18. A. Isser, Subsonic lifting surface model for a blade tip of a hovering helicopter. M.Sc. Thesis, Department of Aeronautical Engineering, Technion, Israel Institute of Technology, Haifa, Israel (1987).
19. H. Multhopp, Methods for calculating the lift distribution of wings (subsonic lifting surface theory). ARC R&M No. 2884 (1950).
20. A. Rosen and A. Isser, Recent studies on the lifting surface theory. *Comput. Math. Applic.* **17**(7), 1115–1130 (1989).
21. C. L. Lawson and R. J. Hanson, *Solving Least Squares Problems*. Prentice-Hall, Englewood Cliffs (1974).
22. A. Rosen and A. Graber, Free wake model of hovering rotors having straight or curved blades. *J. Am. Helicopter Soc.* **33**(3), 11–19 (1988).
23. A. Graber and A. Rosen, A parametric investigation of a free wake analysis of hovering rotors. *Vertica.* **12**(1/2), 179–196 (1988).
24. S. Wagner On the singularity method of subsonic lifting surface theory. *AIAA 7th Aerospace Sciences Meet.*, N.Y., AIAA Paper 69-37 (1969).
25. S. Wagner, Some recent developments in subsonic lifting surface theory. NASA SP-228, pp. 1–35 (1969).